Supporting information

$CsRe_2F_7$@Glass Nanocomposites with Efficient Up-/Down-Conversion Luminescence: from In-Situ Nanocrystallization Synthesis to Multi-Functional Applications

Jiangkun Chen[a,b,c], Shaoxiong Wang[a,b,c], Jidong Lin[a,b,c], Daqin Chen[a,b,c,*]

[a] College of Physics and Energy, Fujian Normal University, Fujian Provincial Key Laboratory of Quantum Manipulation and New Energy Materials, Fuzhou, 350117, China

[*]Corresponding author. E-Mail: dqchen@fjnu.edu.cn

[b] Fujian Provincial Collaborative Innovation Center for Optoelectronic Semiconductors and Efficient Devices, Xiamen, 361005, China

[c] Fujian Provincial Engineering Technology Research Center of Solar Energy Conversion and Energy Storage, Fuzhou, 350117, China

Theoretical calculation laser-irradiation-induced temperature for Er: $CsYb_2F_7$@glass. Based on the Boltzmann distribution theory, UC fluorescence intensity ratio (FIR) of Er^{3+} $^2H_{11/2}$ and $^4S_{3/2}$ thermally coupled states satisfies the following equation:

$$FIR=\frac{I_{525}}{I_{545}}=\frac{g_H A_H \sigma_H w_H}{g_S A_S \sigma_S w_S}\exp(\frac{-\Delta E}{k_B T})=C\exp(\frac{-\Delta E}{k_B T}) \quad (1)$$

where I_{525} and I_{545} are the integrated UC intensities corresponding to the $^2H_{11/2}\rightarrow{}^4I_{15/2}$ and $^4S_{3/2}\rightarrow{}^4I_{15/2}$ transitions of Er^{3+}, respectively, g, A, σ and w are the degeneracy, the spontaneous radiative transition rate, the fluorescence cross-section and the angular frequency of emission transitions from the $^2H_{11/2}$ or $^4S_{3/2}$ excited state to the $^4I_{15/2}$ ground state of Er^{3+}, ΔE is the energy gap of the two thermally coupled states, k_B is the Boltzmann constant, T is the absolute temperature, and C is the constant. Eq. (1) can be expressed as the follow:

$$Ln(FIR)=Ln(C)+(-\frac{\Delta E}{k_B T}) \quad (2)$$

The plot of Ln(*FIR*) versus inverse absolute temperature is linear and the slope ($-\frac{\Delta E}{k_B}$) and intercept ($Ln(C)$) can be determined via the linear fitting of experiment data. According to Eq. (1), FIR alters in terms of temperature while this FIR also depends on laser pumping power, therefore temperature can be correlated with pumping power by the following equation:

$$T=\frac{\Delta E}{k_B[Ln(C)-Ln(FIR)]} \quad (3)$$

where all the parameters have their usual meanings. As a consequence, the temperature in the Er: $CsYb_2F_7$@glass sample induced by laser photothermal effect can be evaluated.

Table S1 Crystallographic data of $CsGd_2F_7$, showing possible 8 cation sites of Gd. The data for the other $CsRe_2F_7$ compounds are similar. [S1]

Atom	X	Y	Z	U_{iso}
Cs1	0.16251(2)	0.08903(2)	0.07580(2)	0.01965(9)
Cs2	0.16784(2)	0.07660(2)	0.42425(2)	0.02243(10)
Cs3	0.35333(2)	0.42573(2)	0.58117(2)	0.01848(9)
Cs4	0.315461(18)	0.416092(18)	0.920588(19)	0.01485(7)
Gd1	0.409549(11)	0.344796(10)	0.220919(13)	0.00585(4)
Gd2	0.407914(11)	0.070520(10)	0.253225(13)	0.00601(4)
Gd3	0.185212(10)	0.341803(10)	0.279355(13)	0.00579(4)
Gd4	0.088215(11)	0.431558(10)	0.746485(13)	0.00575(4)
Gd5	0.090222(11)	0.160077(10)	0.748438(13)	0.00592(4)
Gd6	0.317906(10)	0.158727(10)	0.754130(13)	0.00620(4)
Gd7	0.001401(10)	0.249843(10)	0.492695(12)	0.00648(4)
Gd8	0.499928(11)	0.250234(10)	0.507500(12)	0.00679(4)
F1	0.4205(2)	0.33383(18)	0.03976(19)	0.0176(10)
F2	0.47143(18)	0.10718(16)	0.08637(19)	0.0150(8)
F3	0.11304(19)	0.3092(2)	0.1213(2)	0.0232(10)
F4	0.32105(15)	0.41672(15)	0.15250(17)	0.0098(6)
F5	0.39210(18)	0.19534(15)	0.1770(2)	0.0142(7)
F6	0.24459(16)	0.00391(15)	0.2304(2)	0.0134(7)
F7	0.01106(15)	0.00348(15)	0.2504(2)	0.0124(6)
F8	0.24811(16)	0.24264(16)	0.2515(2)	0.0140(7)
F9	0.05449(16)	0.19118(15)	0.3225(2)	0.0153(7)
F10	0.05165(16)	0.35736(16)	0.3256(2)	0.0133(7)
F11	0.34567(15)	0.41885(15)	0.34517(17)	0.0103(6)
F12	0.4509(2)	0.3160(2)	0.3797(2)	0.0237(12)
F13	0.38632(18)	0.11122(17)	0.4223(2)	0.0171(8)
F14	0.16492(16)	0.33016(20)	0.46060(19)	0.0182(8)
F15	0.03126(19)	0.39133(17)	0.57452(19)	0.0164(8)
F16	0.03442(19)	0.14130(16)	0.57554(19)	0.0165(8)
F17	0.35684(17)	0.35684(17)	0.5848(2)	0.0165(8)
F18	0.16671(16)	0.08251(15)	0.65466(17)	0.0101(6)
F19	0.43925(16)	0.43925(16)	0.6774(2)	0.0161(8)
F20	0.09720(19)	0.29931(16)	0.6926(2)	0.0186(9)
F21	0.09720(19)	0.49515(15)	0.73895(19)	0.0119(6)
F22	0.25433(16)	0.25433(16)	0.7499(2)	0.0123(6)
F23	0.49281(16)	0.49280(15)	0.7778(2)	0.0131(6)
F24	0.0131(6)	0.29690(16)	0.8088(2)	0.0185(7)
F25	0.16355(15)	0.08395(14)	0.84842(16)	0.0095(6)
F26	0.11183(16)	0.39401(16)	0.91592(19)	0.0137(7)
F27	0.11487(16)	0.22308(17)	0.91730(18)	0.0140(7)
F28	0.35557(17)	0.14311(17)	0.92848(19)	0.0166(7)

[S1] K. Friese, N. Khaidukov, A. Grzechnik, Twinned $CsLn_2F_7$ compounds (Ln=Nd, Gd, Tb, Er, Yb): The role of a highly symmetrical cation lattice with an arrangement analogous to the Laves phase $MgZn_2$. Zeitschrift für Kristallographie - Crystalline Materials. 2016, 231, DOI: 10.1515/zkri-2016-1972.

Table S2 Nominal glass compositions (mol%) for all the investigated fluoride-embedded glasses. The samples were prepared by melt-quenching and subsequent heat-treatment at a certain temperature for 2 h. Hexa, cub and orth represents hexagonal, cubic and orthorhombic phases, respectively.

Glass composition (mol%)	Re^{3+} radius (Å)	Crystallizaiton *T*&time	Crystallized phase
$49SiO_2$-$10Al_2O_3$-$12Cs_2O$-15CsF-$14LaF_3$	R_{La}=1.19	700°C/2h	hexa-$CsLa_2F_7$
$49SiO_2$-$10Al_2O_3$-$12Cs_2O$-15CsF-$14CeF_3$	R_{Ce}=1.15	800°C/2h	hexa-$CsCe_2F_7$
$49SiO_2$-$10Al_2O_3$-$12Cs_2O$-15CsF-$14PrF_3$	R_{Pr}=1.14	800°C/2h	hexa-$CsPr_2F_7$
$49SiO_2$-$10Al_2O_3$-$12Cs_2O$-15CsF-$14NdF_3$	R_{Nd}=1.12	800°C/2h	hexa-$CsNd_2F_7$
$49SiO_2$-$10Al_2O_3$-$12Cs_2O$-15CsF-$14SmF_3$	R_{Sm}=1.10	800°C/2h	hexa-$CsSm_2F_7$
$49SiO_2$-$10Al_2O_3$-$12Cs_2O$-15CsF-$14EuF_3$	R_{Eu}=1.09	800°C/2h	hexa-$CsEu_2F_7$
$49SiO_2$-$10Al_2O_3$-$12Cs_2O$-15CsF-$14GdF_3$	R_{Gd}=1.08	900°C/2h	hexa-$CsGd_2F_7$
$49SiO_2$-$10Al_2O_3$-$12Cs_2O$-15CsF-$14TbF_3$	R_{Tb}=1.06	900°C/2h	hexa-$CsTb_2F_7$
$49SiO_2$-$10Al_2O_3$-$12Cs_2O$-15CsF-$14DyF_3$	R_{Dy}=1.05	900°C/2h	hexa-$CsDy_2F_7$
$49SiO_2$-$10Al_2O_3$-$12Cs_2O$-15CsF-$14HoF_3$	R_{Ho}=1.04	950°C/2h	hexa-$CsHo_2F_7$
$49SiO_2$-$10Al_2O_3$-$12Cs_2O$-15CsF-$14YF_3$	R_{Y}=1.04	950°C/2h	hexa-CsY_2F_7
$49SiO_2$-$10Al_2O_3$-$12Cs_2O$-15CsF-$14ErF_3$	R_{Er}=1.03	950°C/2h	hexa-$CsEr_2F_7$
$49SiO_2$-$10Al_2O_3$-$12Cs_2O$-15CsF-$14TmF_3$	R_{Tm}=1.02	950°C/2h	hexa-$CsTm_2F_7$
$49SiO_2$-$10Al_2O_3$-$12Cs_2O$-15CsF-$14YbF_3$	R_{Yb}=1.01	950°C/2h	hexa-$CsYb_2F_7$
$49SiO_2$-$10Al_2O_3$-$12Cs_2O$-15CsF-$14LuF_3$	R_{Lu}=1.00	950°C/2h	hexa-$CsLu_2F_7$
$59SiO_2$-$10Al_2O_3$-$12Cs_2O$-5CsF-$14ScF_3$	R_{Sc}=0.89	750°C/2h	hexa-$CsSc_2F_7$
$55SiO_2$-$6Al_2O_3$-$12Na_2O$-19NaF-$8YF_3$		650°C/2h	hexa-$NaYF_4$
$55SiO_2$-$11Al_2O_3$-$7Na_2O$-19NaF-$8YbF_3$		650°C/2h	cub-$NaYbF_4$
$53SiO_2$-$6Al_2O_3$-$12K_2O$-15KF-$14YbF_3$		750°C/2h	hexa-$KYbF_4$
$41SiO_2$-$6Al_2O_3$-$9K_2O$-19KF-$25YbF_3$		750°C/2h	orth-KYb_2F_7

Table S3 The calculated lattice constants (*a*&*c*) of $CsRe_2F_7$ NCs inside glass based on XRD patterns. The lattice constants show a rise tendency as Re^{3+} radius gradually increases.

Re^{3+}	Sc^{3+}	Lu^{3+}	Yb^{3+}	Tm^{3+}	Er^{3+}	Y^{3+}	Ho^{3+}	Dy^{3+}
R (Å)	0.89	1.00	1.01	1.02	1.03	1.04	1.04	1.05
a (Å)	7.625	7.790	7.806	7.818	7.809	7.910	7.951	8.036
c (Å)	18.571	19.062	19.145	19.170	19.188	19.224	19.287	19.332
Re^{3+}	Tb^{3+}	Gd^{3+}	Eu^{3+}	Sm^{3+}	Nd^{3+}	Pr^{3+}	Ce^{3+}	La^{3+}
R (Å)	1.06	1.08	1.09	1.10	1.12	1.14	1.15	1.19
a (Å)	7.976	8.101	8.108	8.139	8.191	8.297	8.370	8.418
c (Å)	19.404	19.476	19.503	19.611	19.908	19.926	20.052	20.205

Table S4 The calculated temperature (T_c) of Er: $CsYb_2F_7$@glass sample induced by laser irradiation with various power density. As a comparison, the actually measured temperature (T_m) recorded by a laser sight infrared thermometer is provided.

Laser power density (W/cm^2)	FIR	T_c (℃)	T_m (℃)
55	0.701	202	200
95	0.957	282	299
130	1.274	393	366
170	1.634	496	487
195	1.963	635	599
230	2.547	837	825
275	3.001	1154	-

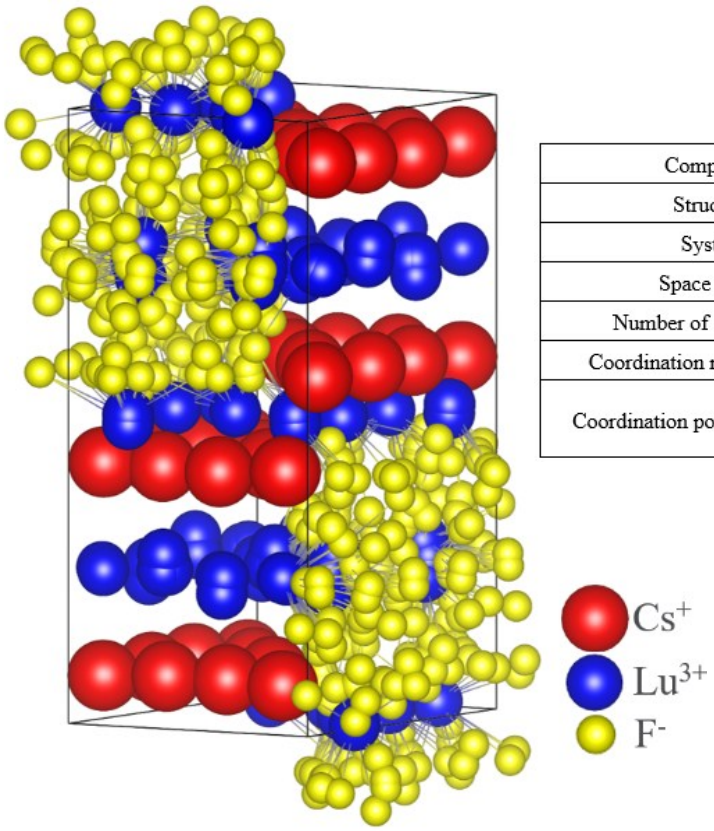

Compound	$CsRe_2F_7$
Structure	$RbEr_2F_7$
System	Hexagonal
Space group	$P6_322$
Number of sites for Re	8
Coordination number for Re	8
Coordination polyhedron for Re	Square antiprism or dodecahedron

Figure S1 Schematic illustration of a typical $CsLu_2F_7$ crystal structure. The ionic sites in the unit cell are tabulated in **Table S1**. Inset is the detailed crystallographic data. [S2]

[S2] V. N. Makhov, N. M. Khaidukov, D. Lo, M. Kirm, G. Zimmerer, Spectroscopic properties of Pr^{3+} luminescence in complex fluoride crystals. Journal of Luminescence, 2003, 102-103, 638.

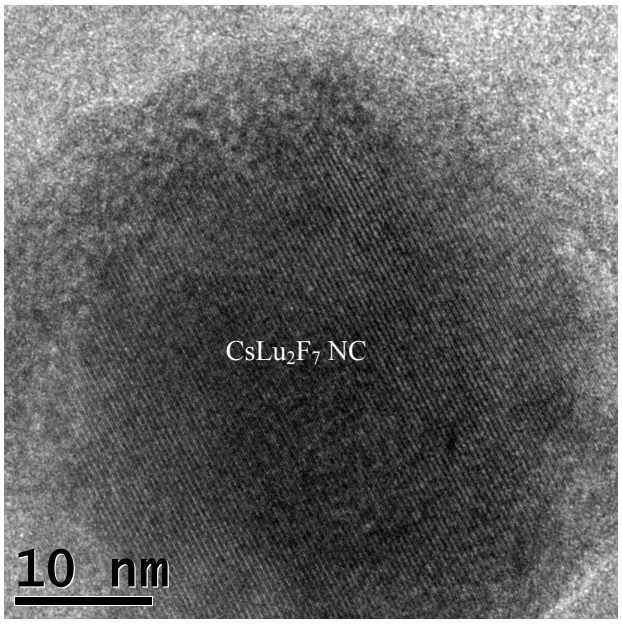

Figure S2 HRTEM image of an individual $CsLu_2F_7$ NC inside glass.

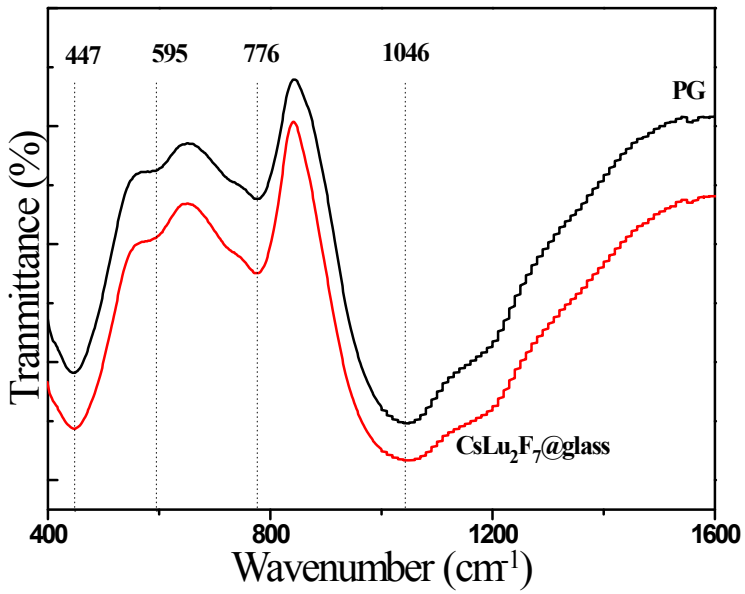

Figure S3 FTIR spectra of precursor glass (PG) and the corresponding $CsLu_2F_7$@glass.

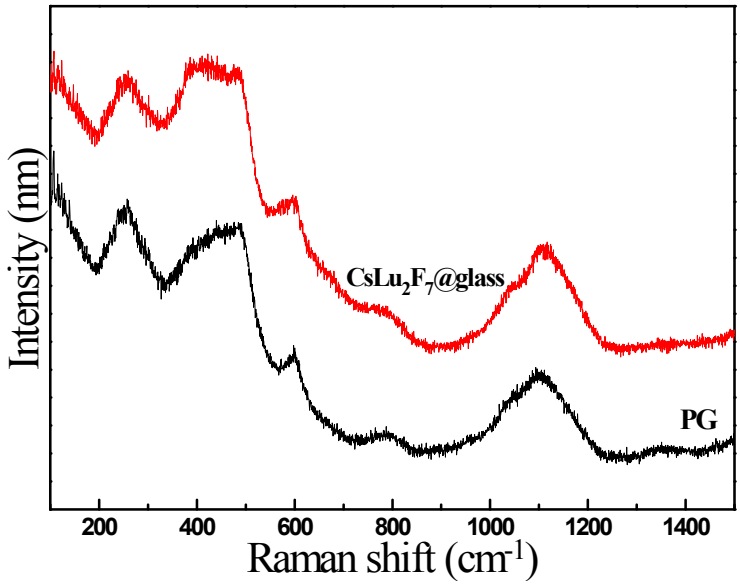

Figure S4 Raman spectra of precursor glass and the corresponding $CsLu_2F_7$@glass.

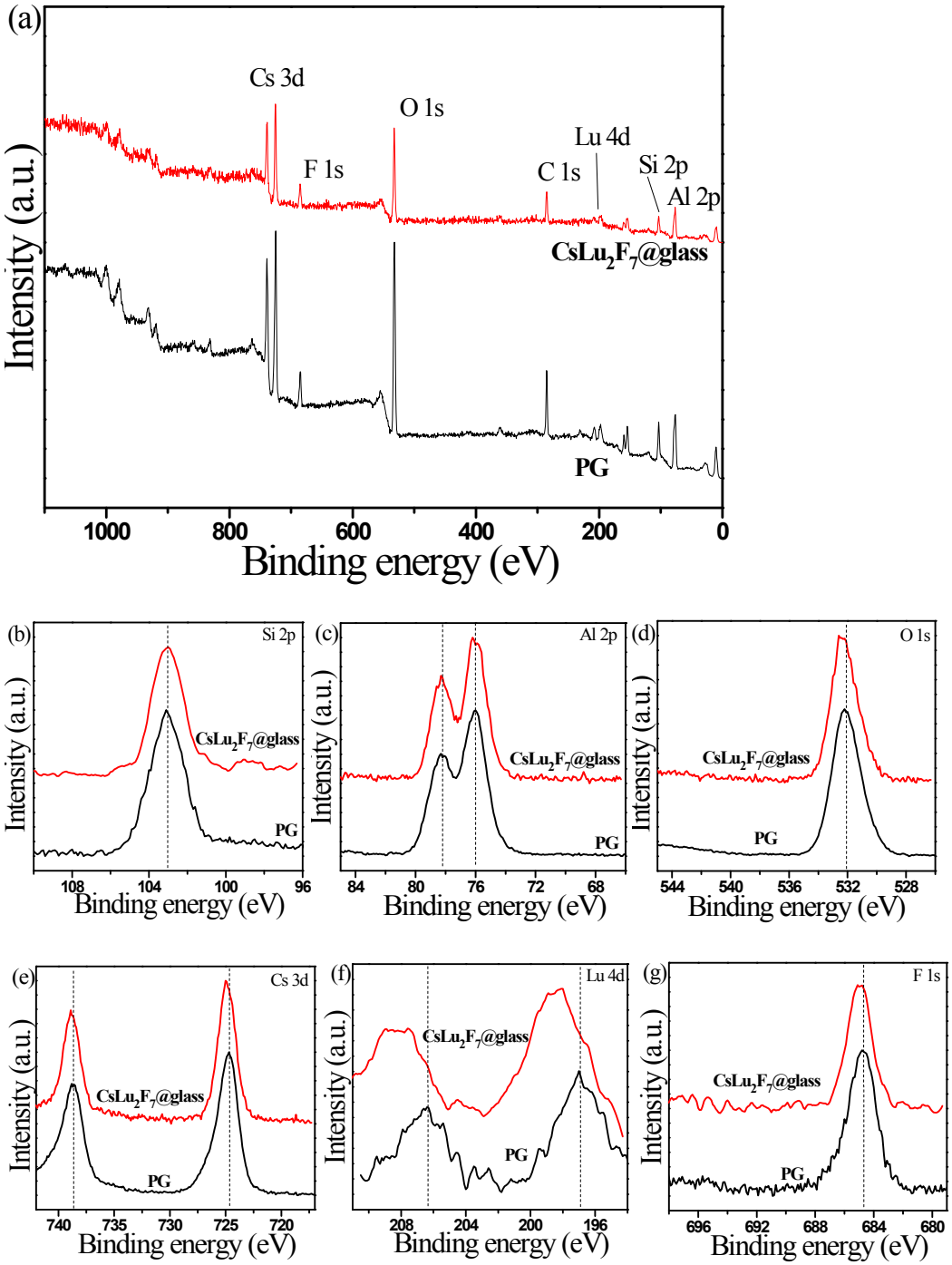

Figure S5 (a) XPS full spectra for precursor glass and the corresponding $CsLu_2F_7$@glass. High-resolution XPS spectra of (b) Si 2p, (c) Al 2p, (d) O 1s, (e) Cs 3d, (f) Lu 4d and (g) F 1s for precursor glass and $CsLu_2F_7$@glass samples.

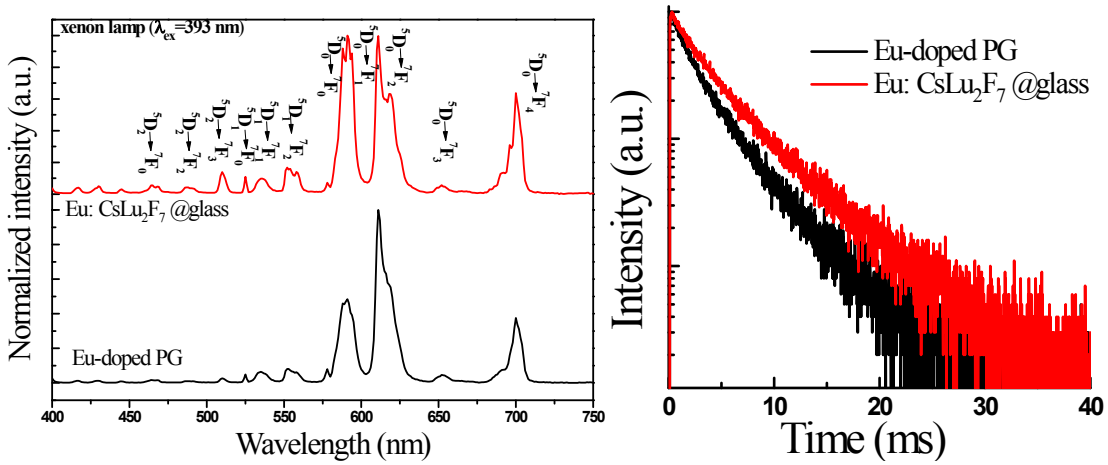

Figure S6 PL spectra and decay curves for Eu-doped precursor glass and Eu: $CsLu_2F_7$@glass.

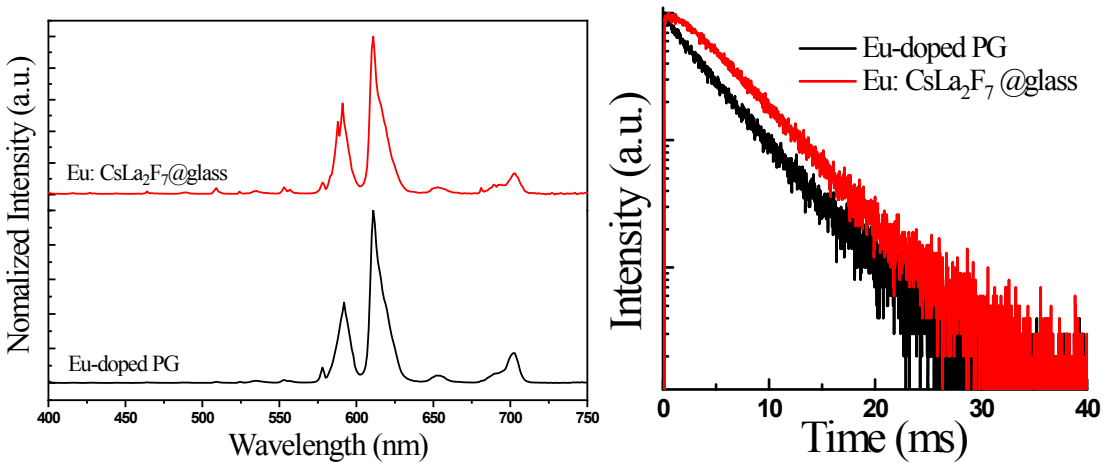

Figure S7 PL spectra and decay curves for Eu-doped precursor glass and Eu: $CsLa_2F_7$@glass.

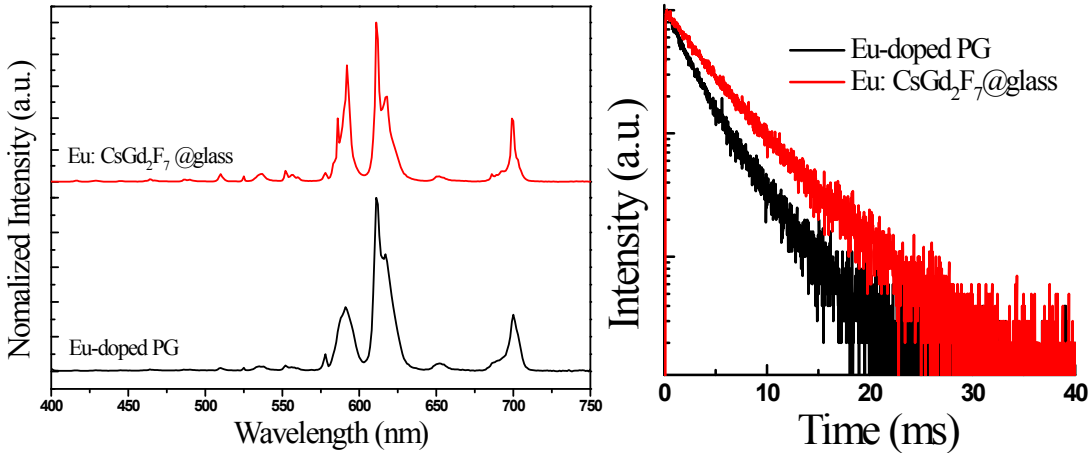

Figure S8 PL spectra and decay curves for Eu-doped precursor glass and Eu: $CsGd_2F_7$@glass.

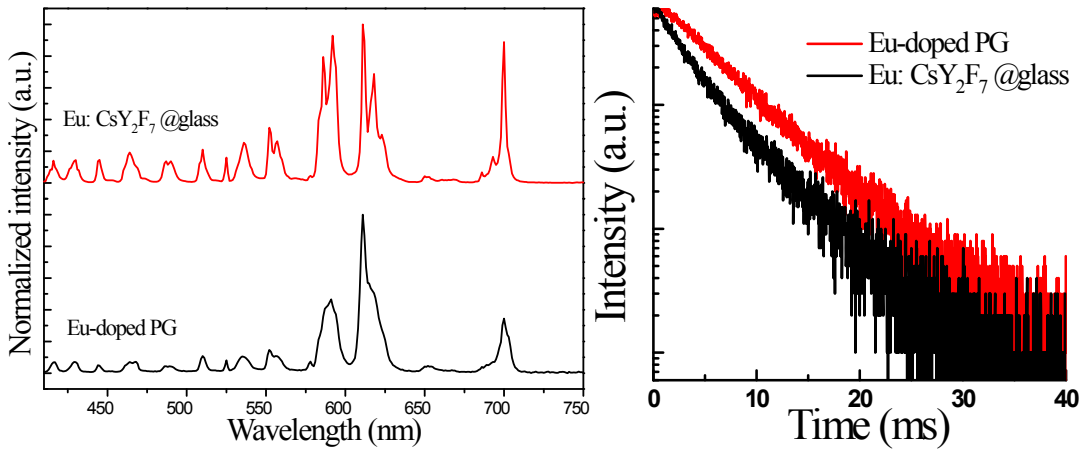

Figure S9 PL spectra and decay curves for Eu-doped precursor glass and Eu: CsY_2F_7@glass.

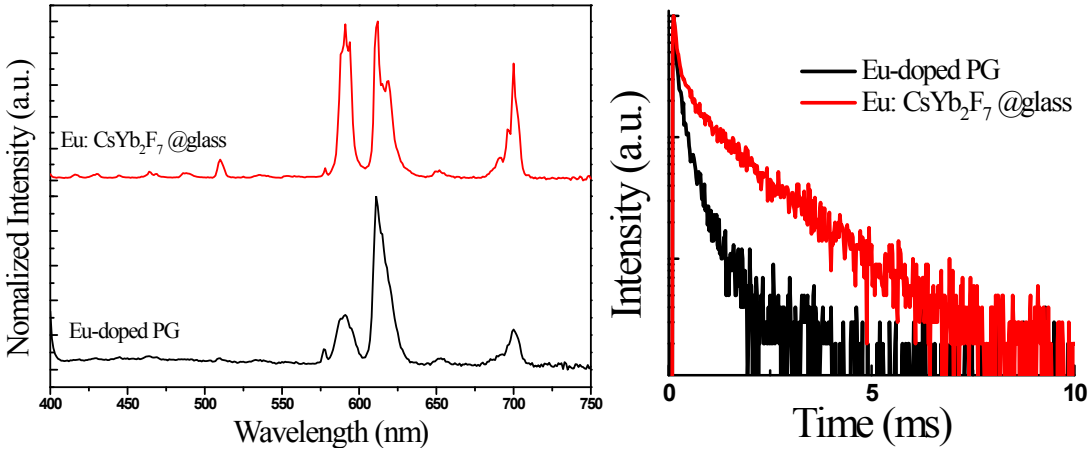

Figure S10 PL spectra and decay curves for Eu-doped precursor glass and Eu: $CsYb_2F_7$@glass.

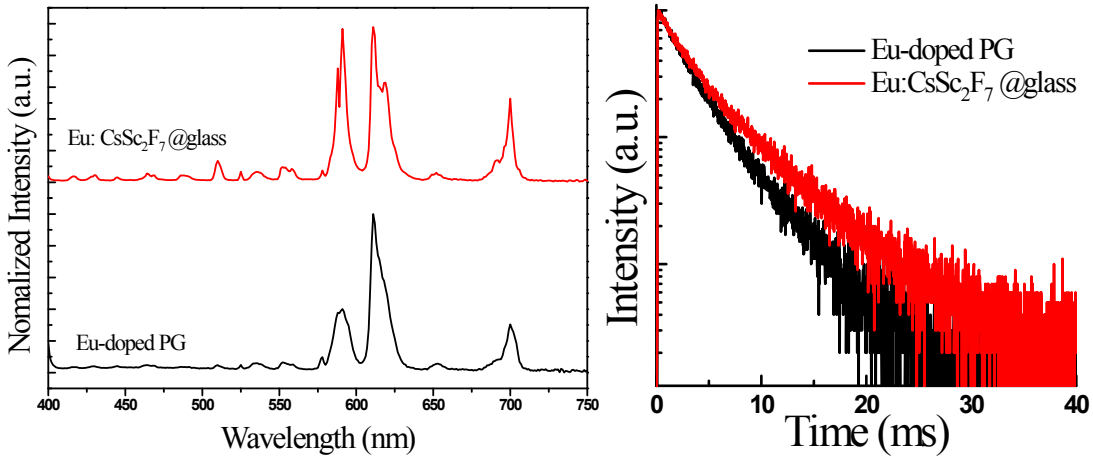

Figure S11 PL spectra and decay curves for Eu-doped precursor glass and Eu: $CsSc_2F_7$@glass.

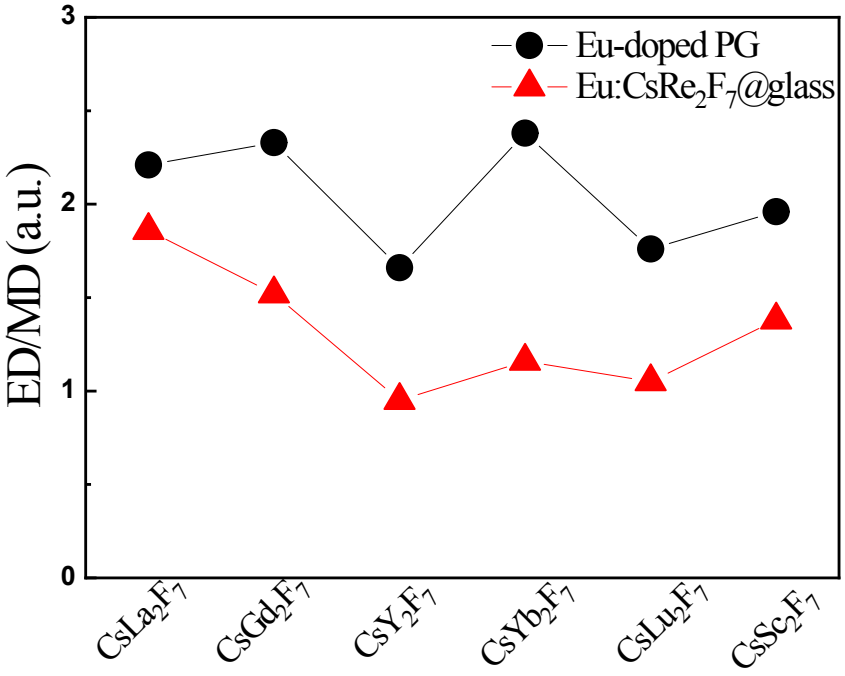

Figure S12 Emission intensity ratio between electric dipolar (ED) $^5D_0 \rightarrow {}^7F_2$ transition and magnetic dipolar (MD) $^5D_0 \rightarrow {}^7F_1$ one for the Eu: $CsRe_2F_7$@glass (Re=La, Gd, Y, Yb, Lu, Sc) samples and the corresponding Eu-doped precursor glasses.

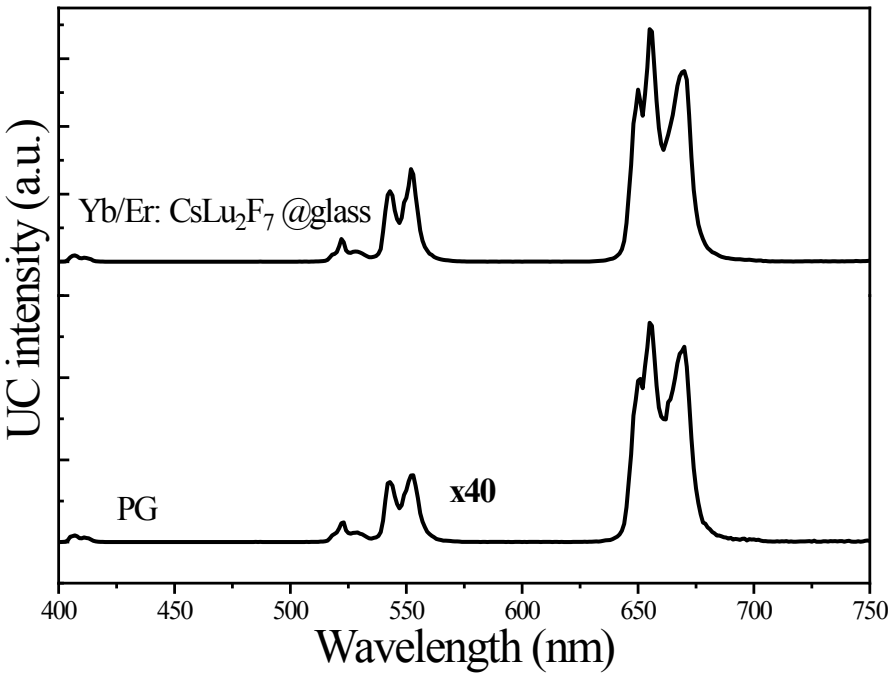

Figure S13 UC emission spectra for Yb/Er-doped precursor glass and Yb/Er: $CsLu_2F_7$@glass.

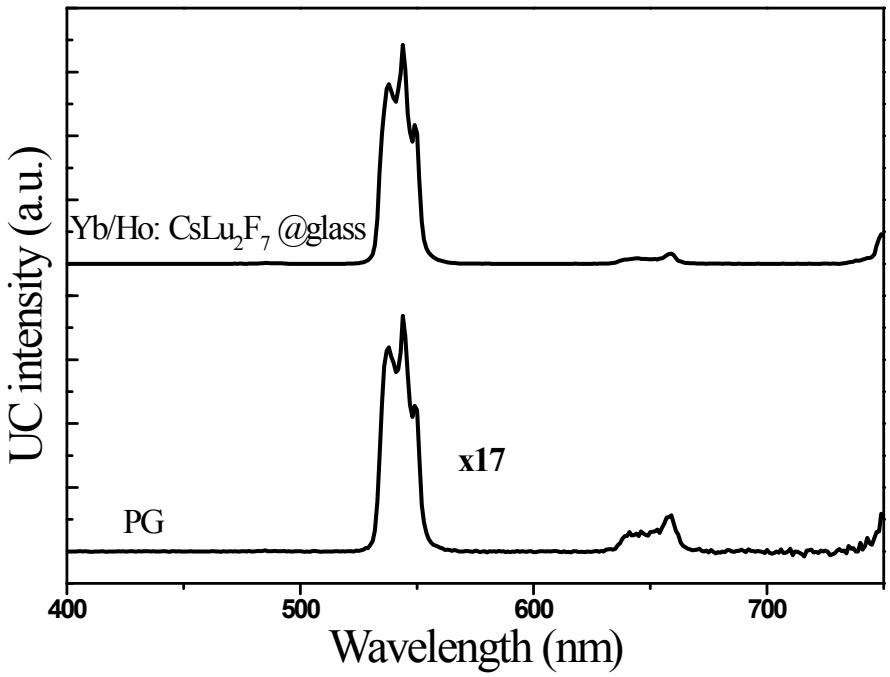

Figure S14 UC emission spectra for Yb/Ho-doped precursor glass and Yb/Ho: $CsLu_2F_7$@glass.

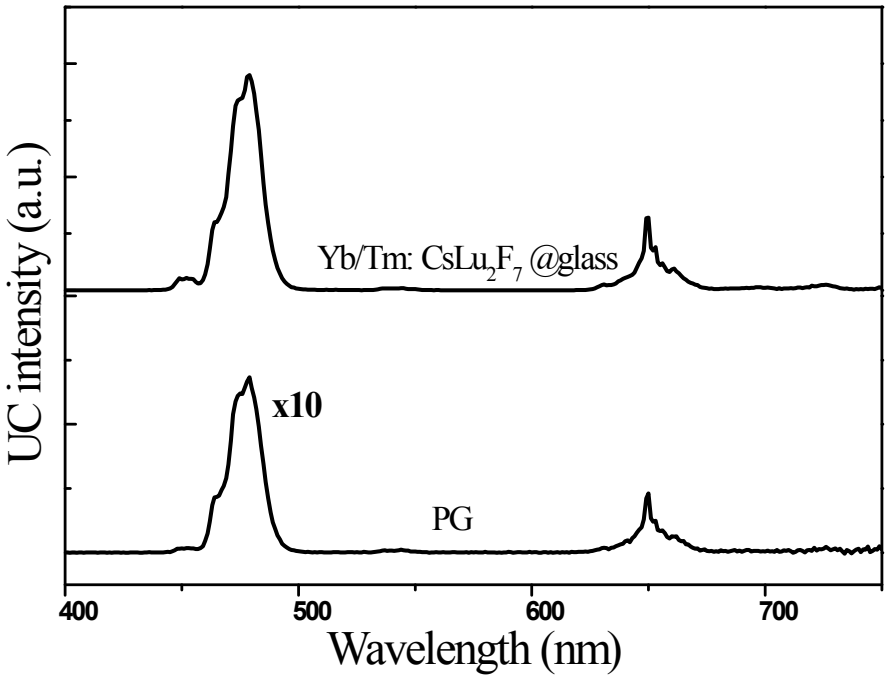

Figure S15 UC emission spectra for Yb/Tm-doped precursor glass and Yb/Tm: $CsLu_2F_7$@glass.

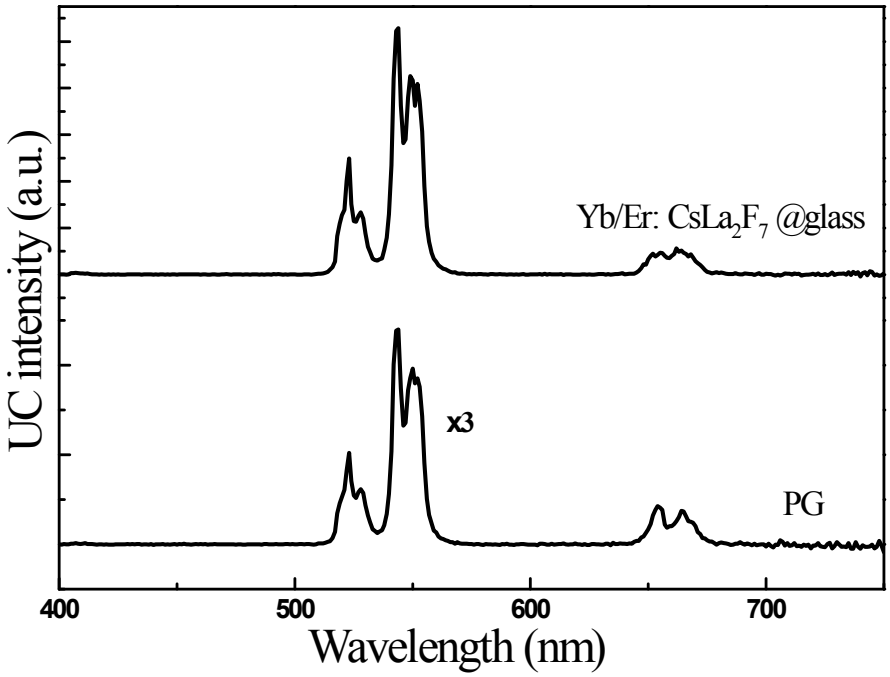

Figure S16 UC emission spectra for Yb/Er-doped precursor glass and Yb/Er: $CsLa_2F_7$@glass.

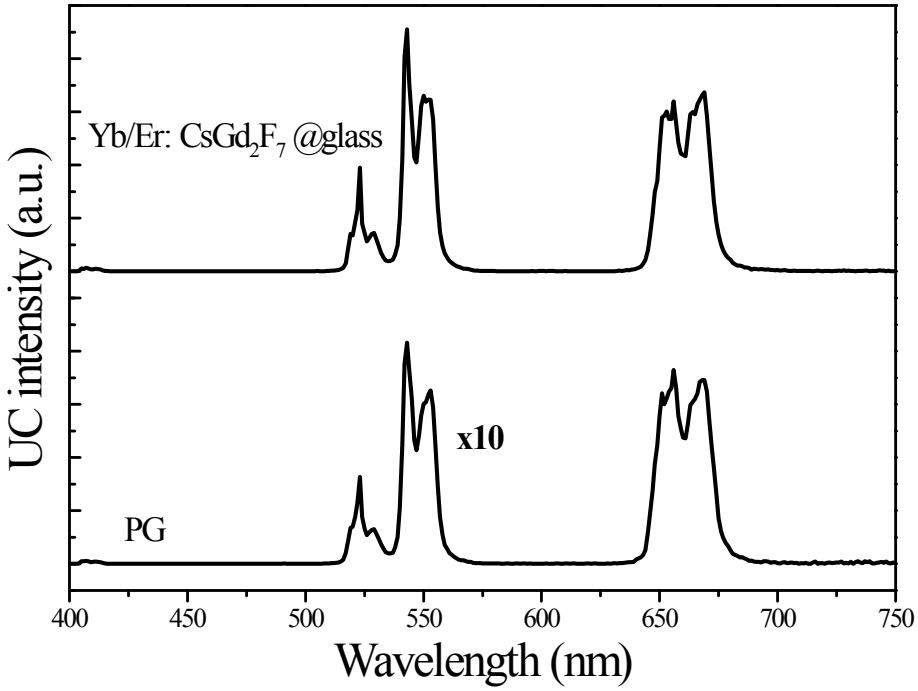

Figure S17 UC emission spectra for Yb/Er-doped precursor glass and Yb/Er: $CsGd_2F_7$@glass.

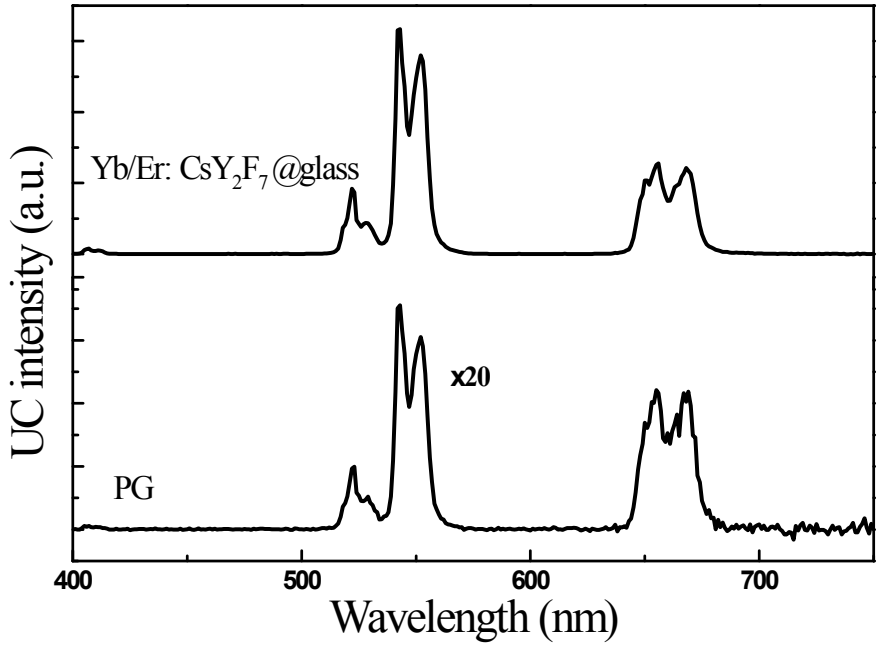

Figure S18 UC emission spectra for Yb/Er-doped precursor glass and Yb/Er: CsY_2F_7@glass.

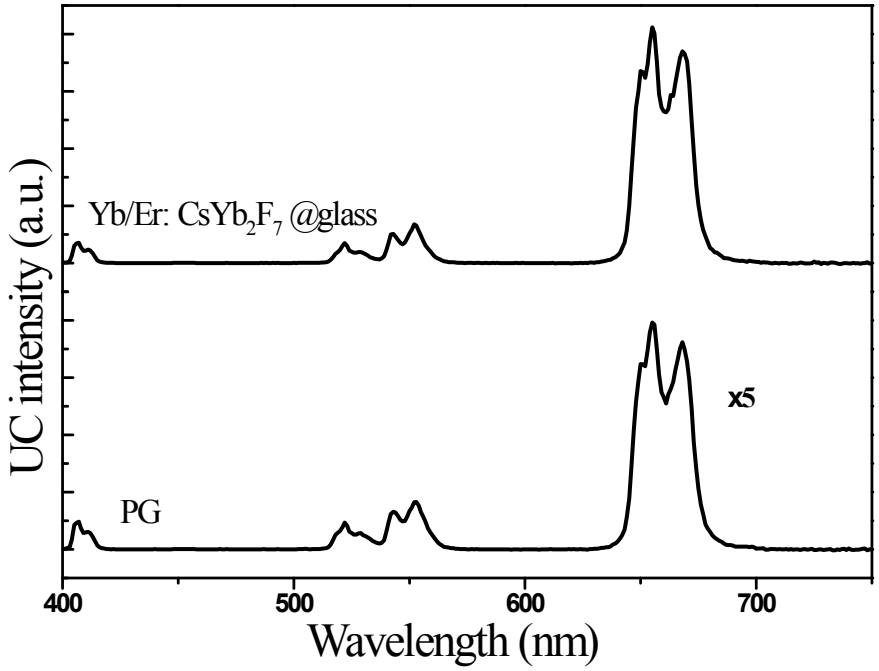

Figure S19 UC emission spectra for Yb/Er-doped precursor glass and Yb/Er: $CsYb_2F_7$@glass.

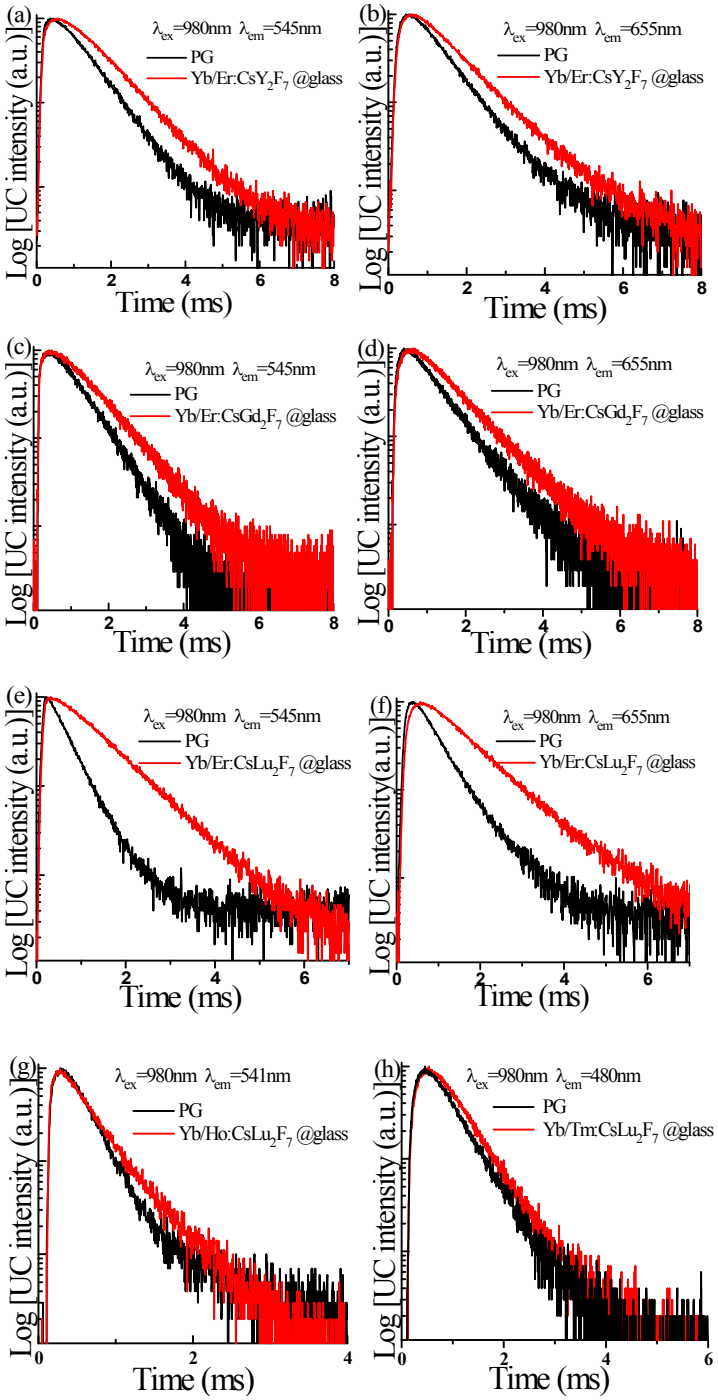

Figure S20 (a-f) UC decay curves for Yb/Er-doped precursor glass and Yb/Er: $CsRe_2F_7$@glass (Re=Y, Gd, Lu) by monitoring Er^{3+} green and red emissions. (g) UC decay curves for Yb/Ho-doped precursor glass and Yb/Ho: $CsLu_2F_7$@glass by monitoring Ho^{3+} red emission. (h) UC decay curves for Yb/Tm-doped precursor glass and Yb/Tm: $CsLu_2F_7$@glass by monitoring Tm^{3+} blue emission.

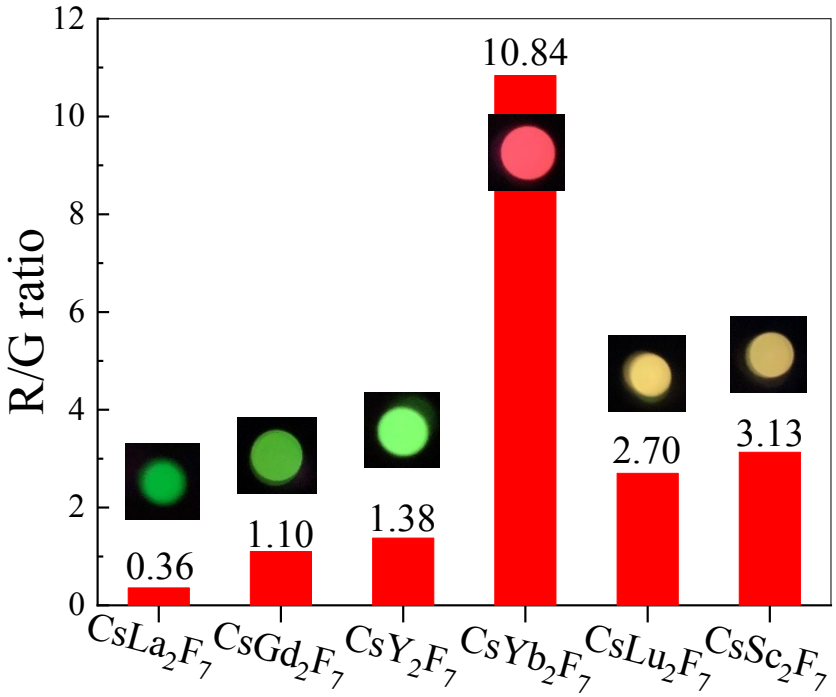

Figure S21 UC red-to-green ratio for Yb/Er: $CsRe_2F_7$@glass (Re=La, Gd, Y, Yb, Lu, Cs) samples. Insets are the corresponding UC emissive photographs under irradiation of 980 nm laser

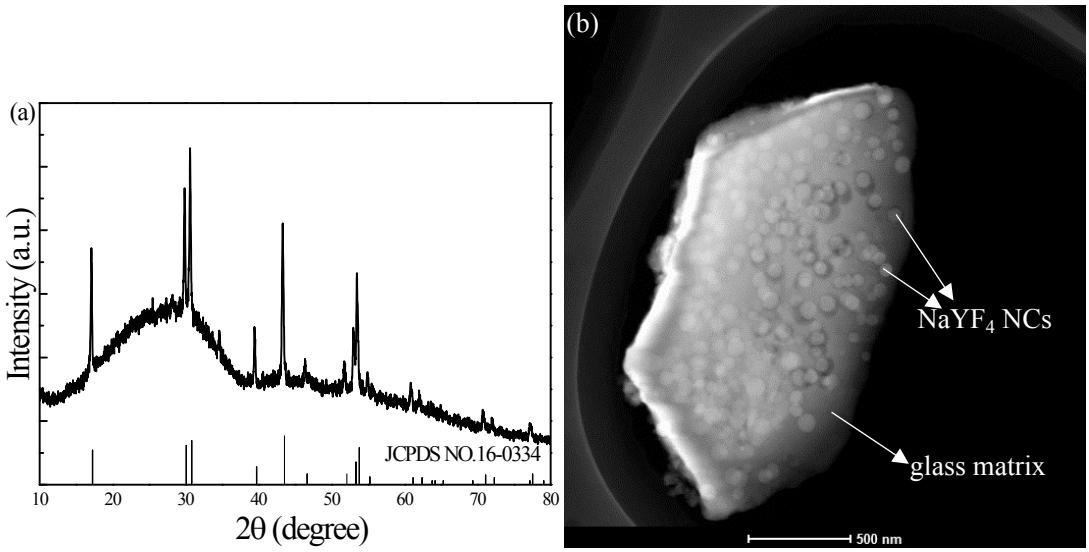

Figure S22 (a) XRD pattern and (b) HAADF-STEM image of Yb/Er: $NaYF_4$@glass sample. Bars represent diffraction data of hexagonal $NaYF_4$ crystal (JCPDS No. 16-0334). The precipitated phase inside glass is hexagonal $NaYF_4$, and the particle sizes are in the range of 40~100 nm.

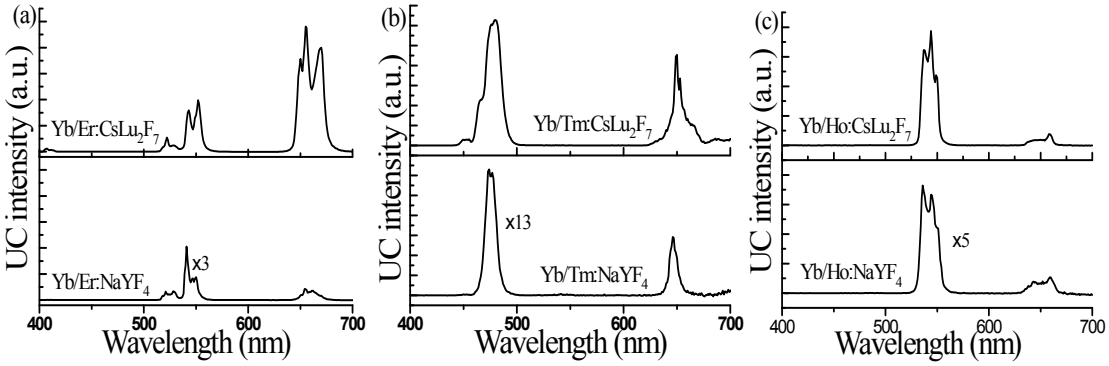

Figure S23 Comparison of UC emission profile and intensity between Yb/Ln: $CsLu_2F_7$@glass and Yb/Ln: $NaYF_4$@glass: (a) Ln=Er, (b) Ln=Tm, (c) Ln=Ho. The corresponding spectra are recorded under the identical conditions.

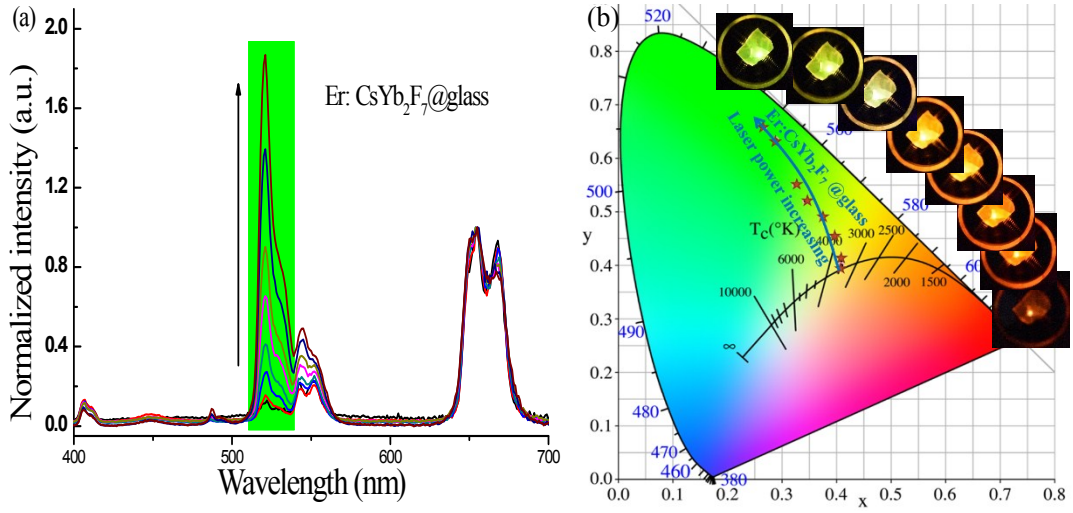

Figure S24 (a) 980 nm laser power density (55~275 W/cm^2) dependent UC emission spectra of Er: $CsYb_2F_7$@glass samples. Arrow represents elevation of laser power density. (b) Color coordinates of UC luminescence for Er: $CsYb_2F_7$@glass in CIE diagram with increase of laser powder density. Insets show remarkable change of UC emissive color for Er: $CsYb_2F_7$@glass samples irradiated by elevated laser power density (from bottom to top).

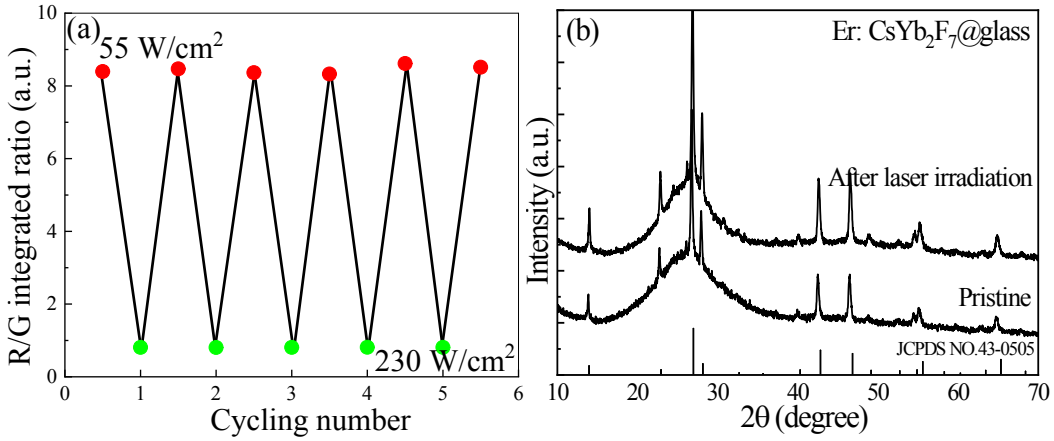

Figure S25 (a) Er^{3+} red-to-green UC emissive ratio for Er: $CsYb_2F_7$@glass in cycles of low laser power density (55 W/cm^2) and high laser power density (230 W/cm^2). (b) XRD patterns of pristine Er: $CsYb_2F_7$@glass and the sample after laser irradiation for 6 cycling times.

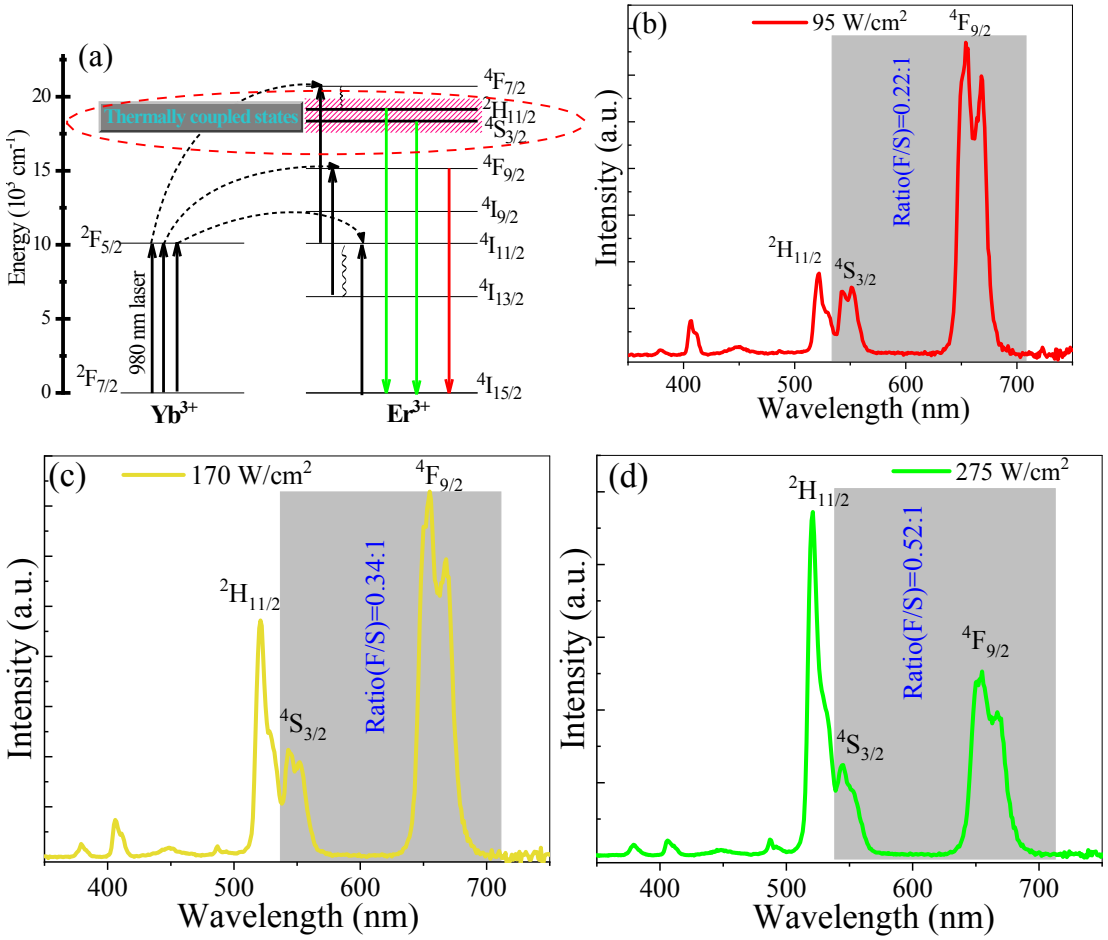

Figure S26 (a) Energy levels of Yb^{3+} and Er^{3+}, Yb-to-Er energy transfer UC processes and Er^{3+} $^2H_{11/2}$ and $^4S_{3/2}$ thermally couple states of in Er: $CsYb_2F_7$@glass. (b-d) Laser power dependent UC emission spectra. The peak ratio between $^4S_{3/2}\rightarrow{}^4I_{15/2}$ transition and $^4F_{9/2}\rightarrow{}^4I_{15/2}$ one is provided.

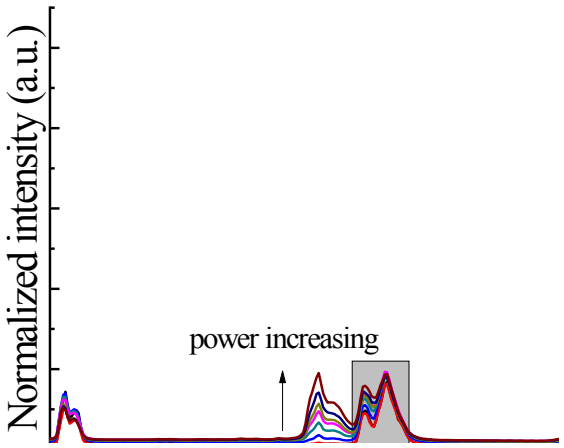

Figure S27 980 nm laser power dependent UC emission spectra of Er: $CsYb_2F_7$@glass recorded at a low temperature (77 K).

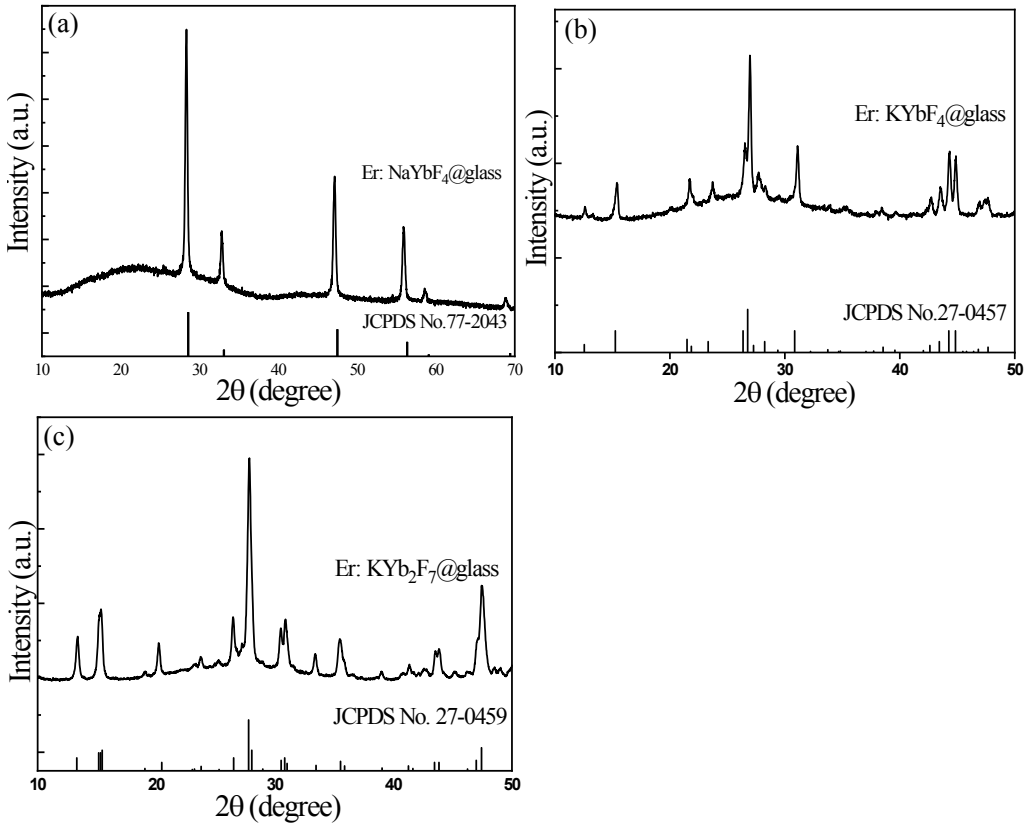

Figure S28 XRD patterns of (a) Er: $NaYbF_4$@glass, (b) Er: $KYbF_4$@glass and (c) Er: KYb_2F_7@glass samples. Bars represent cubic $NaYbF_4$ (JCPDS No. 77-2043), hexagonal $KYbF_4$ (JCPDS No. 27-0457) and orthorhombic KYb_2F_7 (JCPDS No. 27-0459) crystals diffraction data.

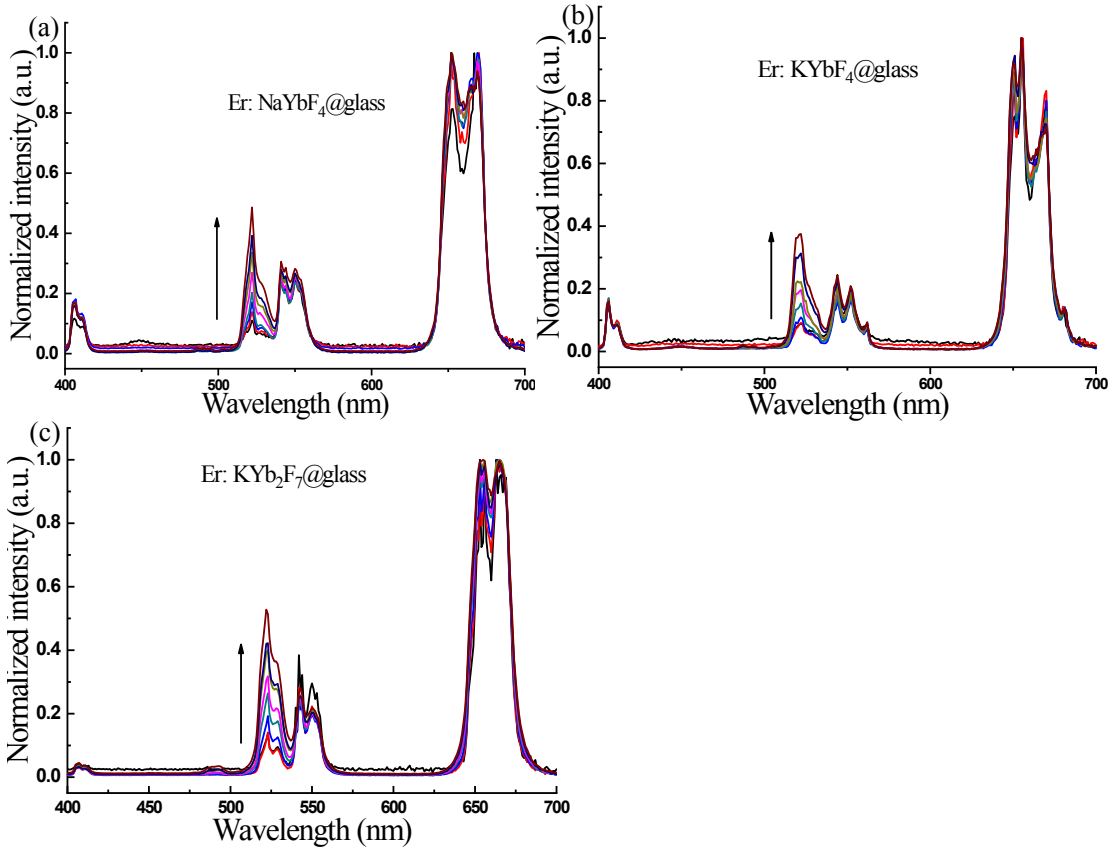

Figure S29 980 nm laser power density (55~275 W/cm^2) dependent UC emission spectra of (a) Er: $NaYbF_4$@glass, (b) Er: $KYbF_4$@glass and (c) Er: KYb_2F_7@glass samples. Arrows represent elevation of laser power density.

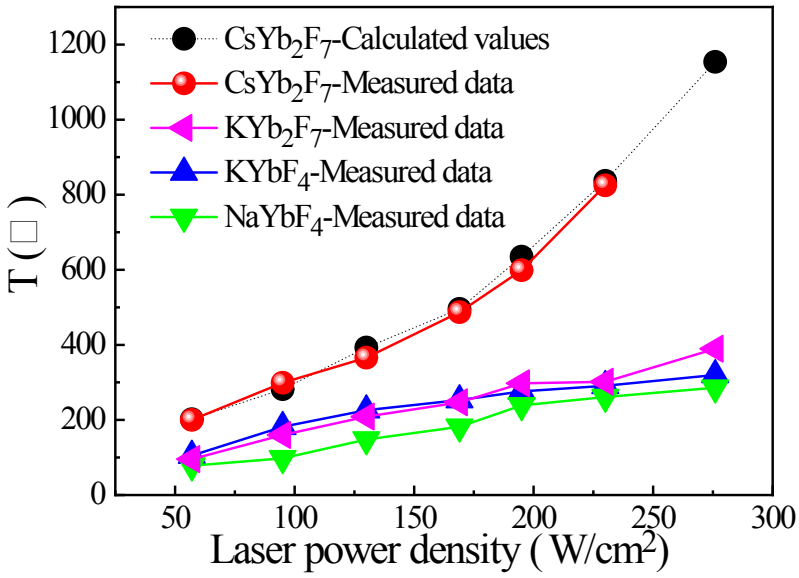

Figure S30 Experimental measured temperatures for the Er: $NaYbF_4$@glass, Er: $KYbF_4$@glass, Er: KYb_2F_7@glass and Er: $CsYb_2F_7$@glass samples exposed to different 980 nm laser power densities. Theoretical calculated temperature values based on repopulation of Er^{3+}: $^2H_{11/2}$ and $^4S_{3/2}$ thermally coupled states for Er: $CsYb_2F_7$@glass are also provided.

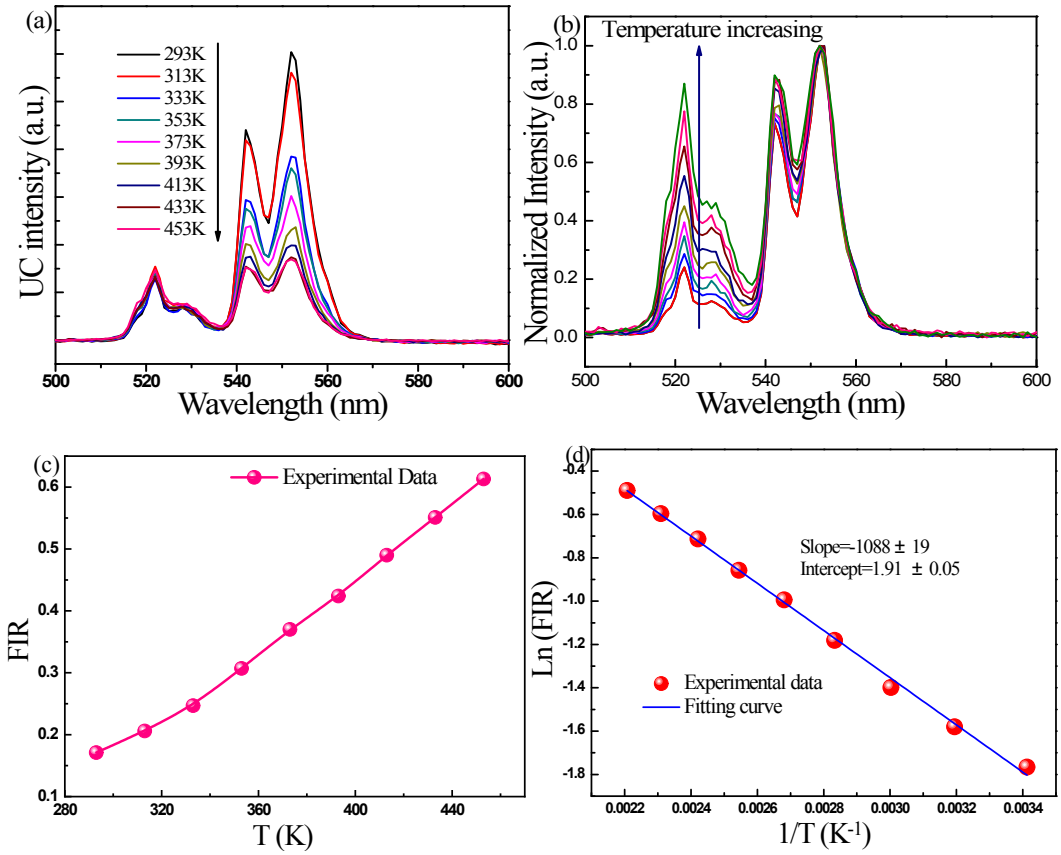

Figure S31 (a) Temperature (313~453 K) dependent UC emission spectra of Er: $CsYb_2F_7$@glass. (b) Normalized UC emission spectra of (a). (c) FIR values versus temperature. (d) Monolog plot of FIR versus inverse absolute temperature. The fitting line is also provided in (d).

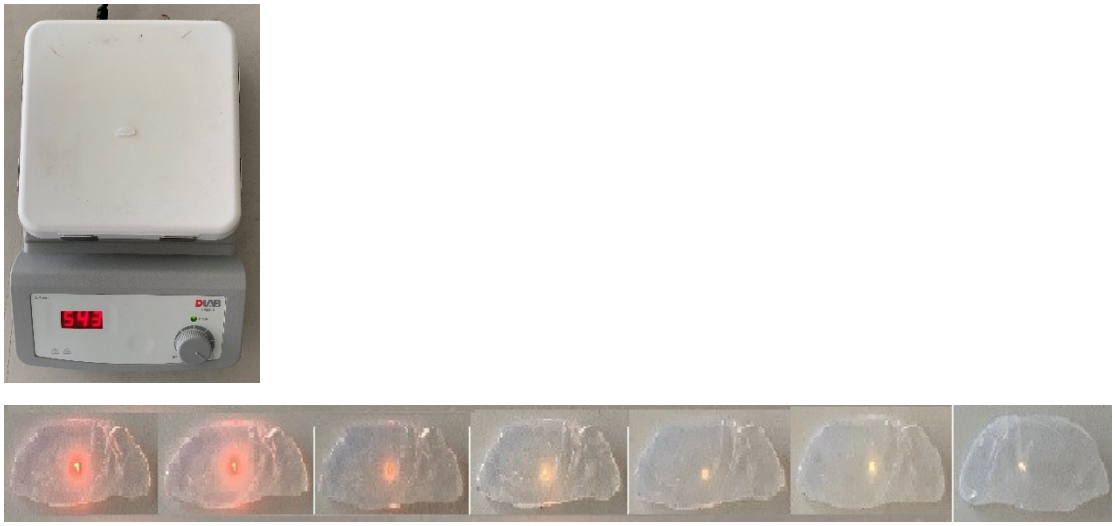

Figure S32 Real-time observation of the change of UC emissive color for Er: $CsYb_2F_7$@glass on a hot plate with elevation of temperature from 30 °C to 550 °C under the irradiation of fixed laser power (500 mW). The temperature of sample from left to right is 30 °C, 100 °C, 200 °C, 300 °C, 400 °C, 500 °C and 550 °C.

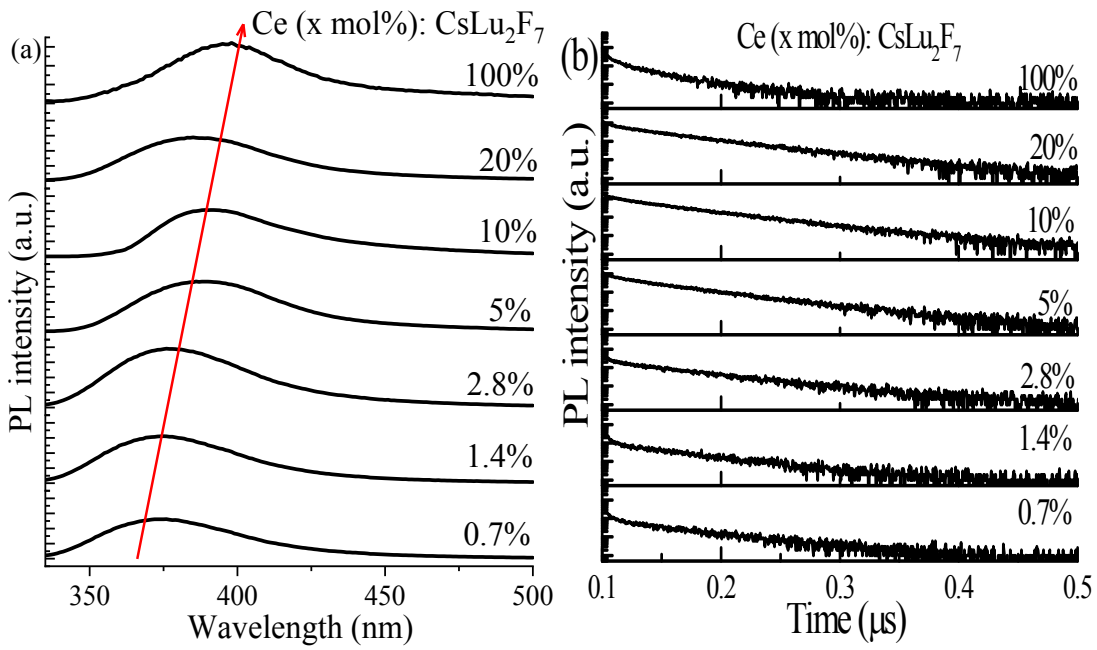

Figure S33 Ce doping content (0.7~100 mol%) dependent PL spectra and decay behaviors for Ce: $CsLu_2F_7$@glass.

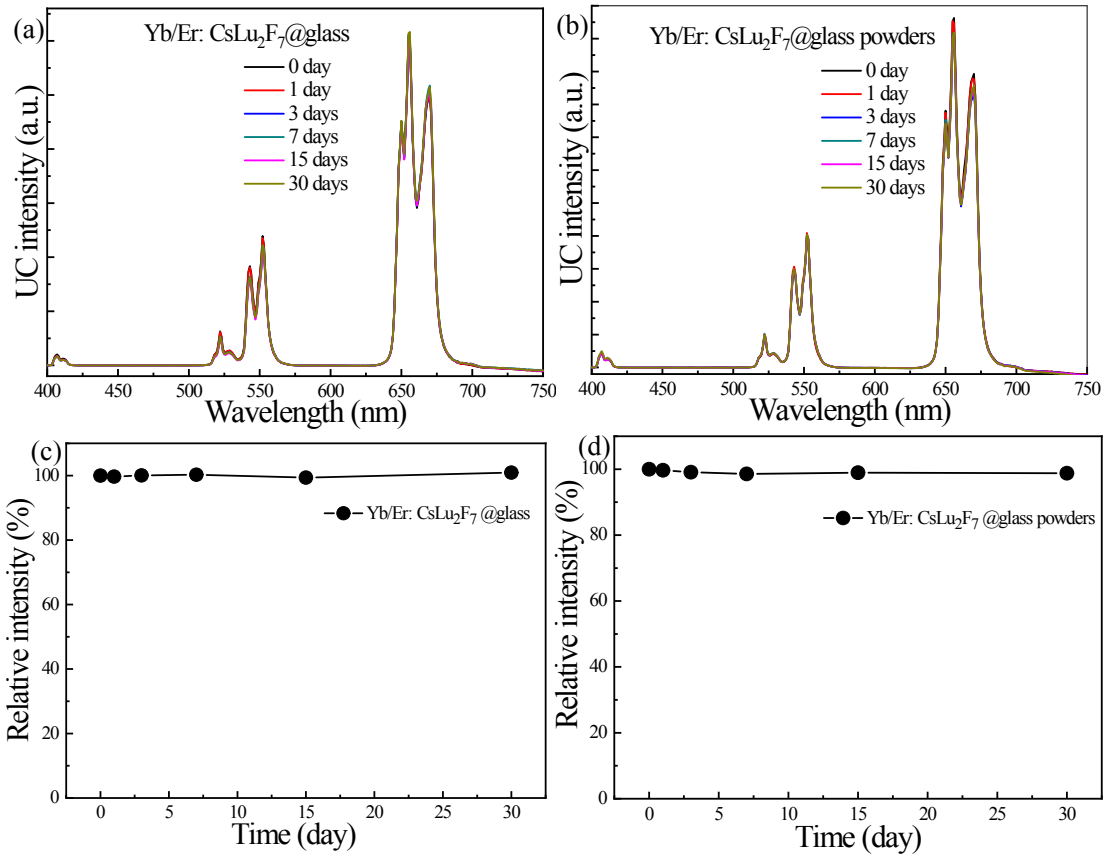

Figure S34 (a, b) UC emission spectra of Yb/Er: $CsLu_2F_7$@glass and the corresponding powders immersing in water for different times (0~30 days). (c, d) UC integrated intensities versus immersing durations in water solution.

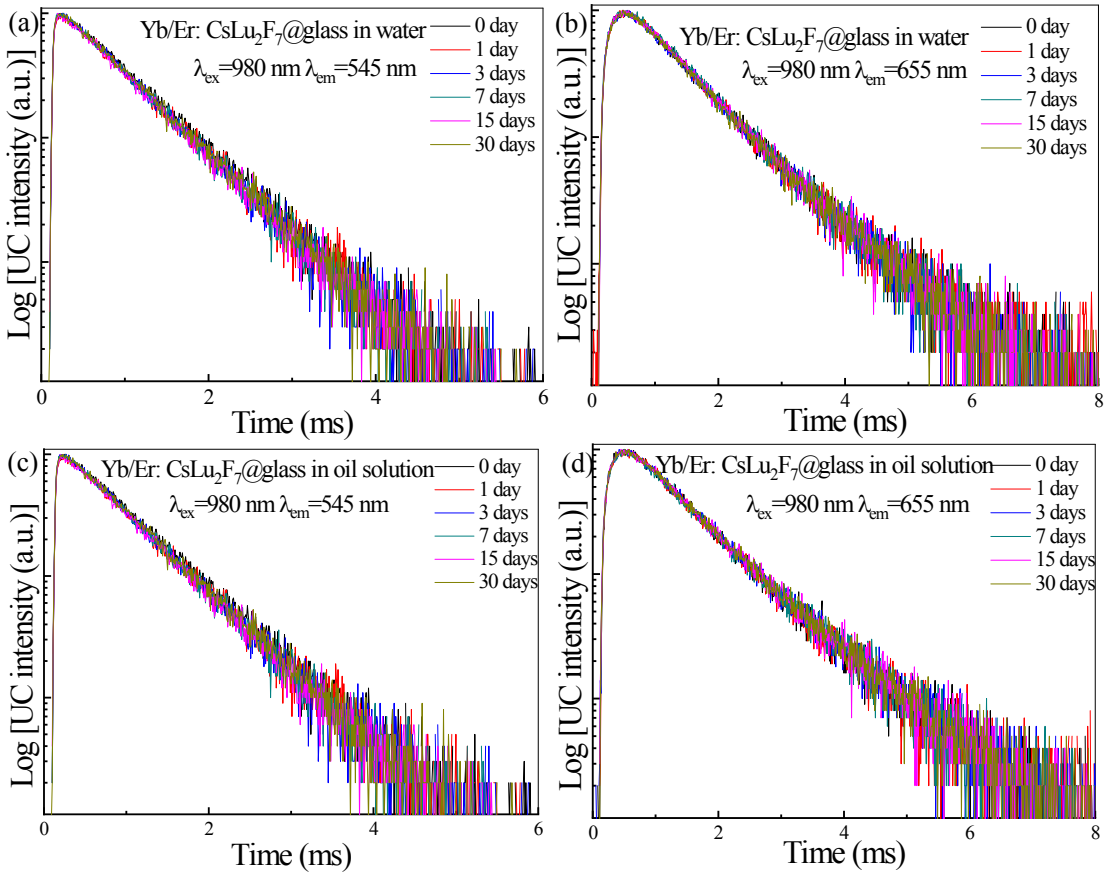

Figure S35 UC decay curves of Yb/Er: $CsLu_2F_7$@glass immersing in solution for different durations (0~ 30 days): (a, b) in water by monitoring Er^{3+} green and red emissions, (c, d) in oil solution by monitoring Er^{3+} green and red emissions.